CALPHAD: Computer Coupling of Phase Diagrams and Thermochemistry 85 (2024) 102692

Contents lists available at ScienceDirect

Calphad

journal homepage: www.elsevier.com/locate/calphad

CALPHAD-based modeling of pressure-dependent Al, Cu and Li unary systems

Elizabeth Mathew [a,*], Rupesh Chafle [a], Benjamin Klusemann [a,b]

[a] Institute of Material and Process Design, Helmholtz-Zentrum Hereon, Max-Planck-straße 1, 21502, Geesthacht, Germany
[b] Institute of Production Technology and Systems, Leuphana University Lüneburg, Universitätsallee 1, 21335, Lüneburg, Germany

ARTICLE INFO

Handling Editor: Prof. Z.K. Liu

Keywords:
Unary system
Thermodynamic assessment
CALPHAD
DFT
High pressure

ABSTRACT

The study presents a pressure-dependent CALPHAD-based model for assessment of the Al, Cu and Li unary systems, focusing on phase changes under varying pressures. By incorporating the Murnaghan equation of state and ab initio phonon calculations, the thermal properties for stable and metastable phases are accurately predicted. To ensure a comprehensive representation of the system's response to pressure changes; compressibility, volumetric thermal expansion coefficient as a function of temperature, the derivative of bulk modulus with pressure, and molar volume for the condensed phases are integrated in the framework. The model provides essential insights into pressure-induced transformation, aiding in the understanding of solid-state processing, such as high-pressure torsion and extrusion. The results from this work are in excellent agreement with the experimental literature and can be utilized to enhance phase predictions under non-equilibrium conditions.

1. Introduction

The development of Al–Cu–Li alloys in the mid 20th century marked a significant advancement in the field of materials science, particularly centered around space, aeronautics and cryogenic applications [1]. This alloy system offers a high strength-to-weight ratio, making them ideal for applications where weight reduction is crucial [2]. However, certain Al–Cu–Li alloys suffer also severe weldability issues [3,4] and show poor ductility and toughness [2,5]. Furthermore, casting such alloys using traditional methods under equilibrium conditions is cumbersome, mainly because liquid Li is highly reactive which leads to ingot cracking [6].

In this regard, to obtain such alloys via different processing routes, one may also employ mechanical alloying, a solid-state processing method carried out under non-equilibrium conditions that aids in the synthesis of novel alloys [7]. The work of Webster et al. [8] demonstrated the use of hot pressing in Al–Cu–Li alloys to overcome the ingot cracking problem during casting. The obtained alloy showed superior strength and lower densities. However, compared to traditional Al alloys, reduced hardness and elongation was observed. Another study by Munoz-Morris [9] showed how equal channel angular pressing (ECAP) can be utilized to increase strength while preserving ductility. It is believed that a fine recrystallized grain structure significantly enhances the mechanical toughness and ductility [10]. Matsumuro and Senoo [11] showed that higher solubility of Li in the Al matrix can be obtained using a high-pressure solid-solution technique, where the supersaturated matrix would nucleate smaller precipitates after subsequent heat treatment. The nucleation rate of precipitates in Al–Cu–Li alloys produced via solid-state processing methods, such as mechanical alloying, extrusion or high-pressure torsion, depends on the specific alloy composition, applied strain, temperature and pressure conditions [9]. Understanding the precipitation phenomena via phase-field modelling and the effect that non-equilibrium conditions that are present during these solid-state processing methods require a knowledge of appropriate thermodynamic databases. Currently, most thermodynamic databases do not consider pressure in their Gibbs energy formulation. The existing CALPHAD-based models that depend on composition and temperature variation alone cannot be utilized to predict the different phases obtained after solid-state processing. Therefore, there is a strong need for the creation of pressure-dependent databases for alloys, such as the Al–Cu–Li system.

The prediction of phase formation at higher pressures requires the consideration of pressure dependency in the formalism of Gibbs energy. Equation of states (EOS) can be used to explain the change in volume as a function of pressure. EOS are empirical relations that define the state of matter [12]. Several EOS ideas have been made by authors such as

* Corresponding author.
E-mail address: Elizabeth.Mathew@hereon.de (E. Mathew).

https://doi.org/10.1016/j.calphad.2024.102692
Received 25 January 2024; Received in revised form 7 April 2024; Accepted 7 April 2024
Available online 23 May 2024

Murnaghan [13], Vinet [14], Brich-Murnaghan [15], and others. The Murnaghan EOS, for example, assumes that the bulk modulus is a linear function of pressure, which has been utilized by various authors [16,17]. Another pressure model based on EOS by Grover et al. has been implemented by Lu et al. [18] in Thermocalc. Lu's model can be extended to higher pressures and is suitable for modelling solution phases [19], however using this model leads to physically impossible heat capacity and entropy values at high pressure, as previously reported by multiple authors [20,21]. Brosh et al. [21,22] tried to address this problem using Mie-Grüneisen EOS [23], considering higher physical contribution over the empirical EOS alongside the Quasiharmonic model, leading to positive heat capacities. For instance, Liu et al. [24,25] utilized Brosh et al. model for Al und Cu successfully, that led to physical thermal expansion values at high pressures above 15 GPa. Joubert et al. [20] used another approach to have a cut-off pressure in Lu's model parameters, namely, integrated volumetric thermal expansion and isothermal compressibility at 1 bar. This method led to a good description of heat capacity for Platinum up to 150 GPa [20]. Huang et al. [26] attempted modeling the molar volume of solution phases for the Al–Cu–Mg system using Lu's model in Thermocalc [18]. Nevertheless, several materials, such as Si, H_2O, Ce and Fe_3Pt that have reported abnormal negative thermal expansion, Liu et al. [27] in their work have explained this from the perspective of thermodynamics by what they refer to as Zentropy theory. They were able to thermodynamically confirm for Ce and Fe_3Pt that the metastable configuration, which replaced the ground stable state, is the cause of the negative thermal expansion by using a multiscale entropy approach. This means that although the volume increases with temperature in the stable state, the decrease in volume is greater for the metastable state that replaced the stable state, leading to the negative thermal expansion.

In this work, the thermodynamic assessment of Al, Cu, and Li, unary systems has been carried out. The scope of the work is limited to 15 GPa. In this regard, the Murnaghan pressure model was utilized with the standard SGTE thermodynamic database for Al, Cu, and Li unary systems [28] to account for the change in volume owing to pressure, which theoretically affects the Gibbs energy. The values of volume, thermal expansion and compressibility were derived from experiments and assessments. Density functional theory (DFT) calculations were also performed to obtain the temperature-dependent volume for face-centered cubic (FCC) lithium phase. All the collected data such as the volume-temperature (V-T), compressibility temperature (κ-T) and thermal expansion temperatures (α-T) data underwent parameter optimization. The obtained unary databases were processed in PyCalphad [29]. Additionally, the Murnaghan pressure model's predictions and the thermophysical characteristics of the stable phase under various pressure conditions obtained via DFT were compared. The assessment can be used to comprehend phase transformation under non-equilibrium settings.

This study is structured as follows. Section 2 provides details about the methodology used and the model taken into consideration. Section 3 describes how the parameters were determined using multiple regression, as well as the details of the unary data utilized for fitting. Section 4 discusses the results, and the key conclusions of this work are highlighted in Section 5.

2. Models

2.1. Murnaghan pressure model

The employed pressure model is based on the formulation of a standard SGTE database [28] with additional contribution from the volume change that occurs due to pressure and temperature. Generally, the pressure dependency of the condensed phase volume may be omitted up to 1 GPa [30]. However, for certain materials like diamond cubic Sn which is only stable below 0.5 GPa, including different contributions is even necessary below 1 GPa [31]. Nevertheless, one must account for the volume change in non-equilibrium cases, especially at high pressures. The Gibbs energy, $G(T, P)$, can be written as [16],

$$G(T,P) = G(T,1) + \int_1^P V(T,P)\,\mathrm{d}P, \tag{1}$$

where $G(T, 1)$ is the Gibbs energy at 1 atm adopted from the SGTE database [28]. There exist several EOS that can extrapolate the experimental volume-pressure results. In this work, the Murnaghan EOS [13] was used to express volume as a function of pressure and temperature given as,

$$V(T,P) = V(T,1)\cdot\left[1 + \frac{nP}{\beta(T)}\right]^{-\frac{1}{n}}, \tag{2}$$

where $V(T, 1)$ and $\beta(T)$ represent the volume and bulk modulus, respectively at 1 atm. The constant n denotes the pressure derivative of the bulk modulus, $\frac{\mathrm{d}\beta}{\mathrm{d}P}$. The volume, $V(T, 1)$ can be written as an integral function of volumetric thermal expansion, α, using the standard thermodynamic relation, see also Appendix A.1,

$$V(T,1) = V_0\,\exp\left(\int_{298.15}^{T} \alpha(T,1)\,\mathrm{d}T\right), \tag{3}$$

where $\alpha = \frac{1}{V}\left[\frac{\partial V}{\partial T}\right]_P$, and V_0 is the volume at 298.15 K and 1 atm. Note that the thermal expansion is written as a function of temperature at 1 atm for an element since the experimental data on molar volume is either obtained at high pressure and room temperature or at high temperature and atmospheric pressure. The following relation is utilized to obtain V_0 and n, see also Appendix A.2,

$$V = \left[\frac{\partial G(T,P)}{\partial P}\right]_T = \frac{V(T,1)}{[1 + nP\kappa(T)]^{1/n}}, \tag{4}$$

where $\kappa(T)$ is the temperature-dependent compressibility function. Numerically, $\kappa(T)$ is the inverse of $\beta(T)$. Using Eq. (2), Eq. (1) can be written after integration as, see also Appendix A.3,

$$G(T,P) = G(T,1) + \frac{V(T,1)}{\kappa(T)(n-1)}\left[\{1 + nP\kappa(T)\}^{\left(1-\frac{1}{n}\right)} - 1\right]. \tag{5}$$

To acquire thermodynamic functions like volume, compressibility, and thermal expansion that were not previously defined in PyCalphad, additional functions were built as extensions in PyCalphad. The process of assessing the unary system is illustrated in Fig. 3.

2.2. Atomistic calculations

Since the thermodynamic quantities for the FCC lithium phase are not available experimentally in the literature, ab initio calculations were performed to determine the thermodynamic parameters of the FCC Li phase. Furthermore, calculated values of the stable phases were compared to experimentally obtained data. Atomic Simulation Environment (ASE) [32] was used to configure all of the calculated structures. DFT-based Vienna Ab initio Simulation Package (VASP) was utilized to perform the calculations. Exchange correlation energy was obtained by using projector augmented wave (PAW) [33] potential with Perdew-Burke-Ernzerhof [34] (PAW-PBE) under generalized gradient approximation (GGA). The initial structure was completely relaxed with respect to the cell's internal and external coordinates. A static ground energy state at 0 K was obtained for Al, Cu and Li structures respectively

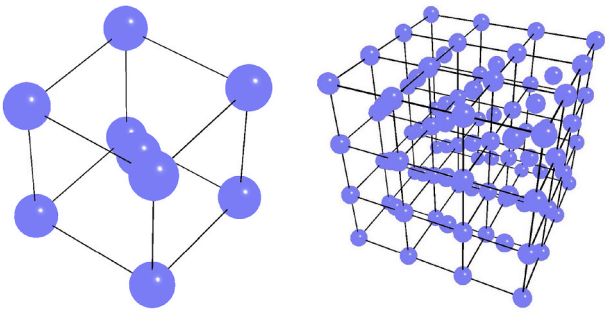

Fig. 1. (a) BCC structure utilized for DFT and MD calculations; (b) 3 × 3 × 3 BCC supercell used for phonopy calculation.

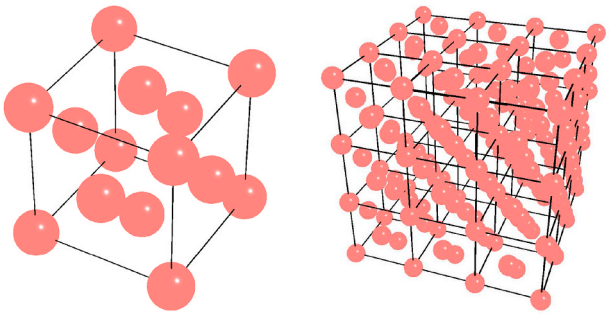

Fig. 2. (a) FCC structure utilized for DFT and MD calculations; (b) 3 × 3 × 3 FCC supercell used for phonopy calculation.

with an energy cut-off of 500 eV. A 30 × 30 × 30 k-point mesh, generated by applying the Monkhorst-Pack scheme, was utilized to sample the Brillouin zone [35]. The convergence of the k-point mesh was checked for high-quality thermodynamic calculations.[1]

The finite displacement method under Harmonic approximation was used to determine thermodynamic parameters such as entropy, S, specific heat capacity, C_p, and Helmholtz free energy, F. The potential energy of a crystal was assumed to be dependent on the displacement of atoms. Another assumption was that every atom in the crystal experiences an increase in force when one of its atoms moves out of its equilibrium position. The second-order force constant with a small displacement in volume was calculated under harmonic approximation to obtain the phonon frequencies. Theoretically, the eigenvalue problem is solved using the second-order energy term and only the real eigenfrequencies were stable. For more details, please refer to Refs. [36–38]. The obtained frequencies under the canonical ensemble were utilized to calculate the Helmholtz free energy. Moreover, C_p and S were obtained using thermodynamic relations. All these transformations are a part of statistical quantum mechanics [37], which is already included as the module 'harmonic' in Phonopy [36]. All computations involving the harmonic approximation were carried out using a supercell of 3 × 3 × 3 and a k-point mesh of 12 × 12 × 12. The computations were conducted using the atomistic structures shown in Figs. 1 and 2.

In the quasi-harmonic approximation (QHA) was used to calculate volume as a function of temperature, assuming that the phonon frequency is volume-dependent. In practice, various volumes are considered and the harmonic approximation is applied to each volume. As an approximation, the Helmholtz free energy, $F(T, V)$ is,

$$F(T,V) \approx U_0(V) + F_{ph}(T,V), \tag{6}$$

where $F_{ph}(T, V)$ is the phonon Helmholtz free energy and $U_0(V)$ is the internal energy calculated from first principles. Using EOS [14], the curves for various temperatures were fitted, and the volume corresponding to the minimum of $F(T, V)$ for each temperature was determined to represent the volume at that temperature. α and β are obtained from calculating equilibrium volume at room temperatures using the relations, $\alpha = \frac{1}{V}\left[\frac{\partial V}{\partial T}\right]$ and $\beta = V\left[\frac{\partial^2 F}{\partial^2 V}\right]$.

For Molecular Dynamics (MD), the embedded atom method (EAM) is a frequently used interatomic potential for metallic materials [39], which was created to better describe the cohesive energy and elastic properties of metals like Al, Cu, and Li. The energy-volume (E-V) curve was fit into the Birch-Murnaghan EOS [15] to acquire the n parameter using MD simulations. LAMMPS Molecular Dynamics Simulator was used to perform MD. The ground state MD calculations were carried out using the EAM potential for Al from Mishin et al. [40], Cu from Mishin et al. [41], and Li from Nicola et al. [42]. The resulting E-V curve was fit into the Birch-Murnaghan EOS [15], see also Appendix A.4.

3. Data

3.1. Aluminium

Al has a FCC structure at atmospheric pressure. It is interesting to note that a transition of FCC → HCP[2] and HCP → BCC[3] was detected using DFT in the early 1960s. Since then, numerous DFT simulations within GGA have validated these transitions at 175 GPa [43–45] and at 360 GPa [44]. However, these transition values couldn't be confirmed experimentally, because shock experiments failed to establish the FCC to HCP transitions [46]. Due to the experimental nature, results are obtained at high temperatures along the Hugoniot. Therefore, any transitions occurring above 150 GPa at room temperature are unlikely to be observed in shock experiments, as the Hugoniot may lead directly to a liquid state, as for instance seen for a BCC → HCP transition for Sn [31]. Later, using a Diamond Anvil cell at 217 GPa, Akahama et al. [47] validated this shift, but at a significantly higher pressure. Recently, Polison et al. [48] using in-situ x-ray diffraction and simultaneous velocimetry measurements, located Al phase transformations, FCC → HCP and HCP → BCC, at 216 ± 9 GPa and 321 ± 12 GPa, respectively. The transitions in the DFT calculations were observed at a lower pressures than experimentally, primarily because the phonon contribution due to temperature is not considered in the free energy calculation.

In the present work, the parameters V_0, n, $\alpha(T)$, and $\kappa(T)$ for the pressure model were formulated and fitted using a combination of experimental and simulated thermodynamic quantities. Thermocouple data from Wilson [49], dilatometer techniques [50,51], as well as data from Pathak and Vasavada [52], were used to determine $\alpha(T)$. Additionally, experimental data from a handbook by Pearson [53], comprising information on thermal expansion, the lattice constant, and molar volume was also used. The assessment by Raju et al. [54] and the model created by Wang et al. [55] are two of the theoretical thermal expansion works used in obtaining $\alpha(T)$.

Tallon et al. [56] derived compressibility data using the piezoelectric oscillator method, while Gerlich and Fischer [57] measured the isothermal compression using ultrasonic wave velocities. Wang and Robert [55] estimated compressibility theoretically using the $\alpha_V K_T V$ model. In this work, the data set by Tallon et al. [56] and Wang and Robert [55] was utilized for our parametrization of $\kappa(T)$.

Given that the experimental data agreed with the model in the work

[1] Calculations of Al and Cu are mainly done for comparison purpose to experimental data as shown in Section 3.4.

[2] HCP = hexagonal closed packed.

[3] BCC = body-centered cubic.

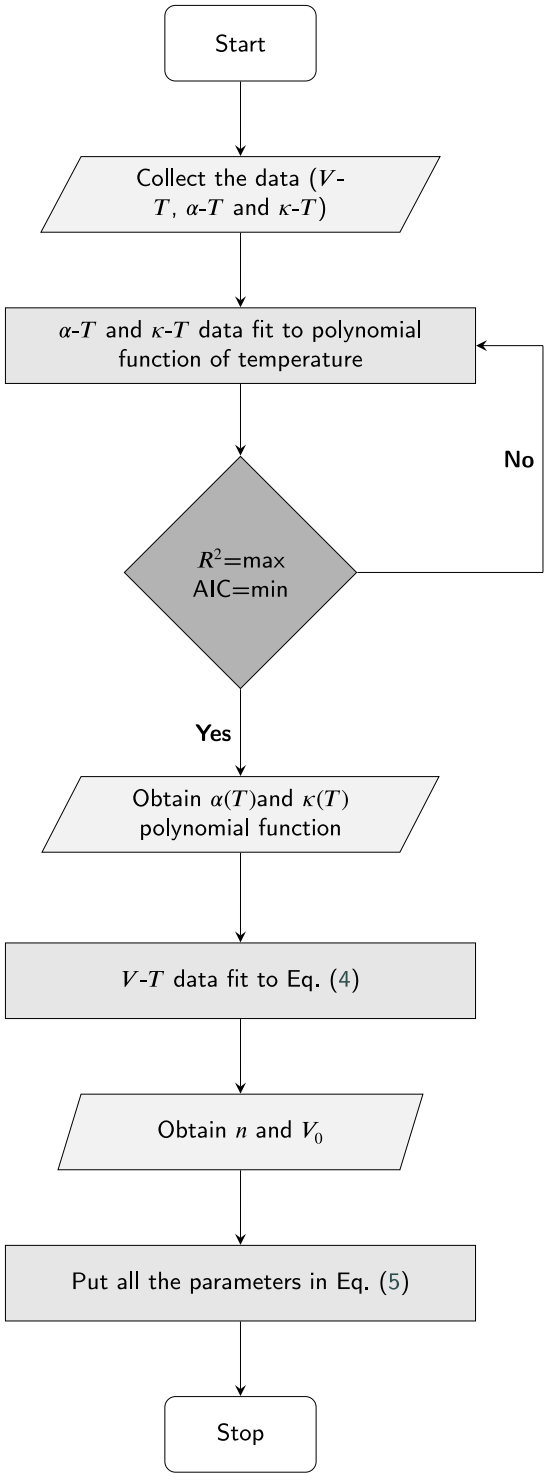

Fig. 3. Flowchart employed for identifying thermodynamic functions and parameters used in this work.

of Wang and Robert [55], volume-temperature data obtained from the model was used to determine the parameters n and V_0. The liquid molar volume data was taken from the sessile drop experiments [58,59] and X-ray attenution results of Smith et al. [60].

The melting curve of aluminium as a function of pressure was considered for validation of the results using diamond anvil cell (DAC) [61–63] and differential thermal analysis techniques by Jayaraman et al. [64]. Moreover, volume pressure data [46,47,62,65–67] was employed to validate the pressure model for the unary system in Section 4.

3.2. Copper

Cu has a FCC structure at atmospheric pressure. There have been no studies that have reported any crystallographic phase transition at different pressures. Thus, FCC and liquid are the only two phases considered.

For the purpose of identifying $\alpha(T)$, thermal expansion experimental data was collected using rotating crystal method by Simmons et al. [68], thermocouples by Leksina and Novikova [69], interferometers by Nix et al. [50], and sensitive methods by Pathak et al. [52].

The bulk modulus data measured by Chang and Himmel [70] by applying ultrasonic pulse-echo, and Overton and John [71] by utilizing cryogenic method, were used to formulate $\kappa(T)$.

To determine n and V_0, the molar volume data as a function of temperature, determined by the X-ray diffraction method adopted by Suh et al. [72] and rotating crystal method applied by Simmons et al. [68], were utilized in this study. For the liquid phase, molar volume data calculated by leviation techniques by Brillo and Evan [73,74] was used. Additionally, the data analysed by Assael [73] was also employed in our work.

Molar volume data as a function of pressure was determined after analysing shock waves by various authors [46,75,76]. Also, data from DAC obtained by Dewaele et al. [66], and high energy synchrotron X-ray diffraction data by Wang et al. [77] was utilized in our work. For liquid Cu, the melting curve as a function of pressure data was collected from Refs. [78,79], they utilized differential thermal analysis techniques and from the work of Brand et al. [80] using a multi-anvil press. The theoretical work of Guinea et al. [81], predicting volume as a function of pressure, was utilized to determine the n parameter for the liquid, as summarized in Table 1.

Table 1
Assessed parameters of unary Al, Cu and Li.

Element	Phase	Parameters
Al	FCC	$V_0 = 9.7801 \times 10^{-6}$ $\alpha(T) = 6.2065 \times 10^{-5} + 1.6824 \times 10^{-8}\,T + 3.7630 \times 10^{-11}\,T^2$ $\kappa(T) = 1.3094 \times 10^{-11} - 4.9641 \times 10^{-16}\,T + 5.9247 \times 10^{-18}\,T^2$ $n = 3.5$
	liquid	$V_0 = 9.9190 \times 10^{-6}$ $\alpha(T) = 1.5243 \times 10^{-4} - 4.07107 \times 10^{-8}\,T$ $\kappa(T) = 1.8105 \times 10^{-11}$ $n = 4$
Cu	FCC	$V_0 = 6.9832 \times 10^{-6}$ $\alpha(T) = 4.7183 \times 10^{-5} + 7.6327 \times 10^{-9}\,T + 1.2707 \times 10^{-11}\,T^2$ $\kappa(T) = 7.0051 \times 10^{-12} + 1.2377 \times 10^{-15}\,T + 1.2242 \times 10^{-18}\,T^2$ $n = 4.5$
	liquid	$V_0 = 6.9850 \times 10^{-6}$ $\alpha(T) = 1.004 \times 10^{-4} - 1.0918 \times 10^{-9}\,T + 6.8581 \times 10^{-13}\,T^2$ $\kappa(T) = 5.925 \times 10^{-14} + 9.377 \times 10^{-15}\,T + 1.2242 \times 10^{-20}\,T^2$ $n = 5$
Li	BCC	$V_0 = 1.2565 \times 10^{-5}$ $\alpha(T) = 4.4652 \times 10^{-5} + 4.2318 \times 10^{-7}\,T - 3.3707 \times 10^{-10}\,T^2$ $\kappa(T) = 8.0517 \times 10^{-11} - 1.5327 \times 10^{-14}\,T + 1.3282 \times 10^{-16}\,T^2$ $n = 2.79$
	FCC	$V_0 = 1.2410 \times 10^{-5}$ $\alpha(T) = 1.0069 \times 10^{-4} + 8.1369 \times 10^{-8}\,T + 6.7976 \times 10^{-11}\,T^2$ $\kappa(T) = 7.8641 \times 10^{-11} - 1.4327 \times 10^{-14}\,T + 1.2182 \times 10^{-16}\,T^2$ $n = 2.67$
	liquid	$V_0 = 9.919 \times 10^{-6}$ $\alpha(T) = 1.9005850991 \times 10^{-4} + 9.8756 \times 10^{-8}\,T$ $\kappa(T) = 1.0417 \times 10^{-11} + 1.2327 \times 10^{-14}\,T + 5.05821 \times 10^{-16}\,T^2$ $n = 4.1$

3.3. Lithium

Lithium is a prime example of a nearly-free electron metal at atmospheric pressure where the valence electrons barely interact with the atomic cores [86]. Following the identification of low symmetry phases in a combined experimental and theoretical research [87,88], lithium under pressure has shown a variety of complicated characteristics, including superconductivity [89,90], and a significant minimum in the melting curve at around 190 K [91]. Lithium adopts a BCC structure at room temperature and shows a transition from BCC → FCC at 7.5 GPa. At low temperatures and high pressure, FCC and $R\bar{3}m$ space group structures are present [88]. Since the SGTE first-generation CALPHAD database starts from room temperature, the structures are restricted to BCC, FCC and liquid in the present calculations. Moreover, the P-T diagram up to 20 GPa was plotted, as the experimental results are scarce beyond that.

The volume-temperature data for BCC Li phase were obtained from the work of Anderson and Swenson [92] using piston displacement techniques, as well as from the works [93,94] utilizing DAC. Thermal expansion data [95–97], compressibility-temperature data [92,98] using the piston displacement technique and also from the theoretical work of Dologlou [99] were considered as well. Volume-pressure data was taken from Hanfland et al. [94] and Frost et al. [93].

Since not much data for the FCC phase was available, the volume temperature, thermal expansion temperature and bulk modulus temperature data were calculated using Phonopy. The available volume-pressure data [93,94] was utilized for determining the n and V_0 parameters.

3.4. Comparison of parameter n obtained through different approaches

Since, the quality of the obtained thermodynamic parameters is directly linked to the quality of the employed data, it is advisable to validate the individual parameters by employing different methods. In Table 2, the parameter n determined via experimental data is compared with MD and DFT results, obtained by fitting the static E-V curve from these calculations, see also Appendix A.4. Overall, the experimental fit exhibits close agreement with both MD and DFT results. It is evident that the parameter n obtained from MD simulation is closer to the experimental fit results than DFT. Since MD utilizes EAM potentials, which are derived from theoretical and experimental results, it is understandable that the MD is closer to the experimentally determined results in this study.

4. Results and discussion

In this section, the state variables and thermodynamic quantities derived from unary assessments are compared to available experimental and theoretical values. The obtained final parameters are shown in Table 1.

4.1. Al unary system

The pressure-temperature (P-T) phase diagram for the Al unary system is shown in Fig. 4. The resulting thermodynamic assessment led to a good fit for the majority of experimental data. However, at higher pressure, the model begins to underestimate the temperature. Liu et al.

Table 2
Parameter n obtained via fitting the experimental results to Eq. (4) and validating by E-V data obtained via MD and DFT.

Element	Structure	Expt. fit	MD	DFT
Al	FCC	3.5	3.7	4.6
Cu	FCC	4.5	5.0	4.3
Li	BCC	2.8	2.8	3.3

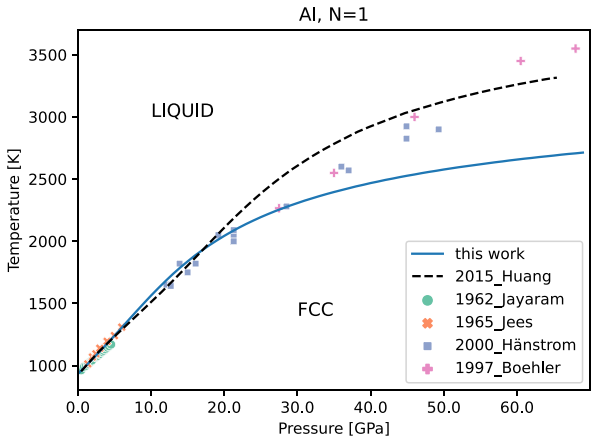

Fig. 4. Al pressure-temperature phase diagram obtained using the evaluated thermodynamic data from Table 1. Symbols indicate the corresponding literature data [61–64].

[24] reported a comparable issue when employing a Lu-Grover's EOS for Al. The reason in this work is due to the Murnaghan pressure model used that produces the unphysical heat capacities of the phases at higher pressure, see also Appendix A.5. A comparison with the assessment by Huang et al. [26], who employed Lu's model, shows that both assessments resulted in slightly different responses, but still similar good agreement to the experimental data up to 30 GPa. Fig. 5 displays the thermophysical properties obtained via the Murnaghan pressure model for four different pressures, i.e., 1 atm, 1 GPa, 2 GPa and 5 GPa. Fig. 5 (a) illustrates the specific heat capacity as a function of temperature. This has also been compared to the specific heat capacity results obtained via QHA. Both results report a decrease in the heat capacity as the pressure increases. The ambient pressure C_p computed by the model is in good agreement with the experimental results [100–106]. The calculated α as a function of temperature is presented for the stable FCC Al phase in Fig. 5 (b). The obtained α values were compared with all the available experimental values. The results are in good agreement with existing works [49–55]. The pressure model exhibits a drop in α at higher pressures, which is in good agreement with the QHA estimate. However, the model shows a qualitative disagreement, while the QHA model predicts a monotonous increase of the thermal expansion with temperature, the Murnaghan model predicts that at a higher pressure of 5 GPa for some temperature ranges, the thermal expansion decreases with temperature. Moreover, the Murnaghan pressure model has been compared to Hallstedt [85] thermal expansion results that were obtained for ambient pressure by formulating molar volume as a function of temperature. The volume as a function of temperature is shown in Fig. 5 (c). The obtained volume with the pressure model were compared with the experimental work Wang and Robert [55] and theoretical work of Hallstedt [85]. The QHA volume is slightly overestimated for different pressures, which is related to the fact that DFT calculations are performed at 0K. In this regards, the results are extrapolated for higher temperatures but we ignore temperature-dependent energies. Moreover, under these approximations, it is assumed that the volume is dependent only the phonon frequencies. Temperature dependence of β is presented in Fig. 5 (d). The calculated β is in close agreement with other works [26,55,56]. There was an increase in β with pressure. Only the bulk modulus QHA compuation at 0 GPa is plotted, because it was not possible to acquire the accurate bulk modulus at any other pressure under this approximation.

Fig. 6 (a) shows the molar volume as a function of temperature up to 1200K for FCC and liquid Al phases. A comparison has been made with the experimental results of [55,58–60]. The model slightly underestimates the volume from the experiments and the work of Huang

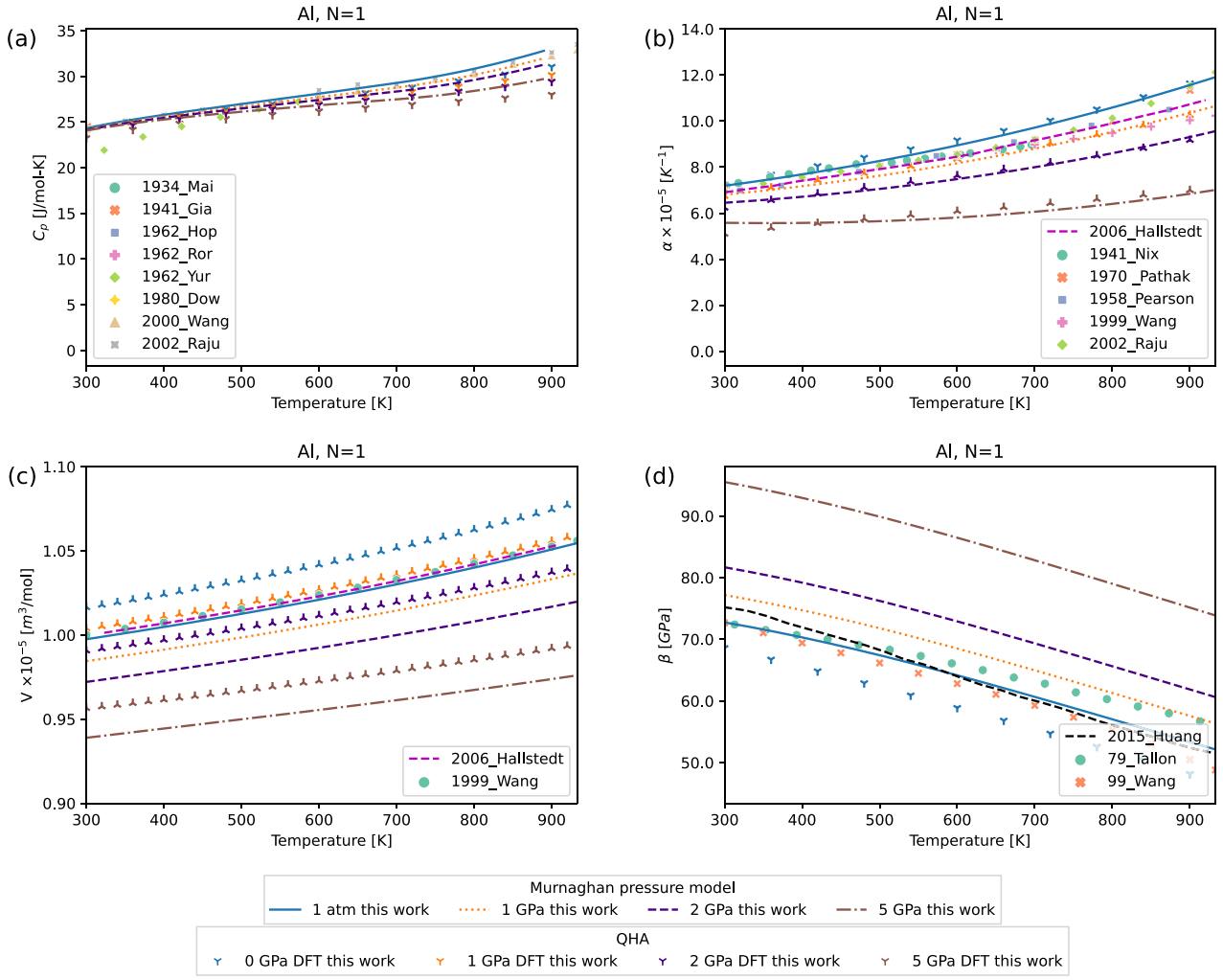

Fig. 5. Temperature-dependent thermophysical properties of FCC Al determined using the Murnaghan pressure model and QHA calculations at various pressures: (a) Specific heat capacity at constant pressure (C_p), with literature data measured at 1 atm [54,55,82–84]. (b) Volumetric thermal expansion (α), compared to literature data at 1 atm [49–55,85]. (c) Measured molar volume, where the literature data is taken from Refs. [55,85]. (d) Bulk modulus (β) as a function of temperature, with data measured at atmospheric pressure [26,55–57].

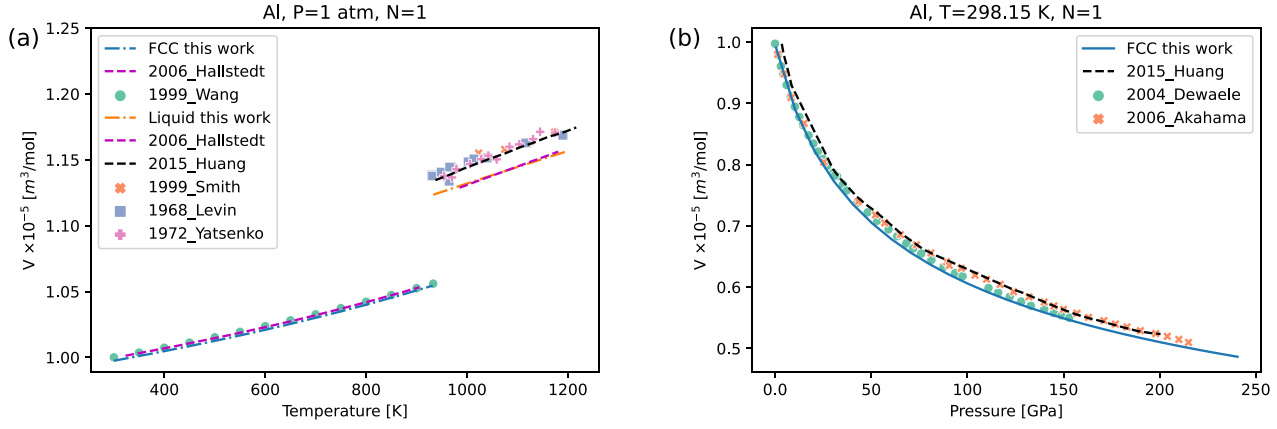

Fig. 6. Thermodynamic properties of unary Al: (a) Measured molar volume as a function of temperature at atmospheric pressure, where the literature data is taken from Refs. [26,55,58,59,85]. (b) Calculated molar volume at room temperature with literature data [26,47,66].

et al. [26]. However, an agreement can be seen with Hallstedt [85] molar volume calculations Fig. 6 (b) shows the molar volume as a function of pressure up to 2.5 GPa at room temperature for the FCC Al phase. The volume-pressure function obtained closely reproduces the experimental results by Dewaele et al. [66] and Akahama et al. [47], as well as Lu-Grover's EOS model work of Huang et al. [26].

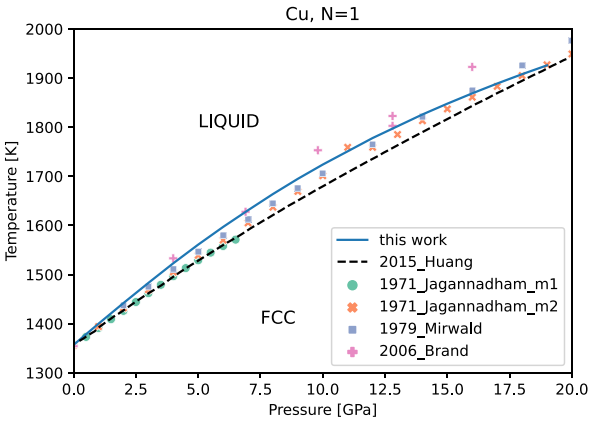

Fig. 7. Cu pressure-temperature phase diagram obtained using the evaluated thermodynamic data from Table 1. Symbols indicate the corresponding literature data [78–80].

4.2. Cu unary system

The P-T phase diagram of the unary Cu system is displayed in Fig. 7 for comparison together with earlier evaluation findings from Huang et al. [26] and specific data sets obtained from experiments [78–80]. The current work accurately reproduces the experimental findings.

Fig. 8 illustrates the thermophysical properties obtained via the pressure model for four different pressures, namely at 1 atm, 5 GPa, 10 GPa and 15 GPa. Fig. 8 (a) shows C_p with respect to temperature. Similar to Al, Cu also shows a decrease in the C_p as a function of pressure, which is also evident in the QHA. The model's computation of ambient pressure C_p closely matches the experimental findings [100–106]. In Fig. 8 (b) the computed α as a function of temperature is shown for the stable FCC Cu phase. All of the available experimental results were compared with the resulting α values. The obtained results are in good agreement with previous research [50,52,68,69]. Additionally, the model has been compared to thermal expansion results for ambient pressures derived by Lu et al. [107]. At higher pressures, the model shows a decline in α, which is more consistent with the QHA estimate. However, QHA computed α results are not in complete agreement with the present model, since the temperature-related effects might not be fully accounted for via DFT calculations, as mentioned already earlier. Furthermore, at greater pressures of 15 GPa, the Murnaghan pressure model still predicts the monotone increment indicated by the QHA model. However, the thermal expansion decreases with temperature. Fig. 8 (c) displays the volume as a function of temperature. The Murnaghan pressure model was compared with experimental [68,72] and

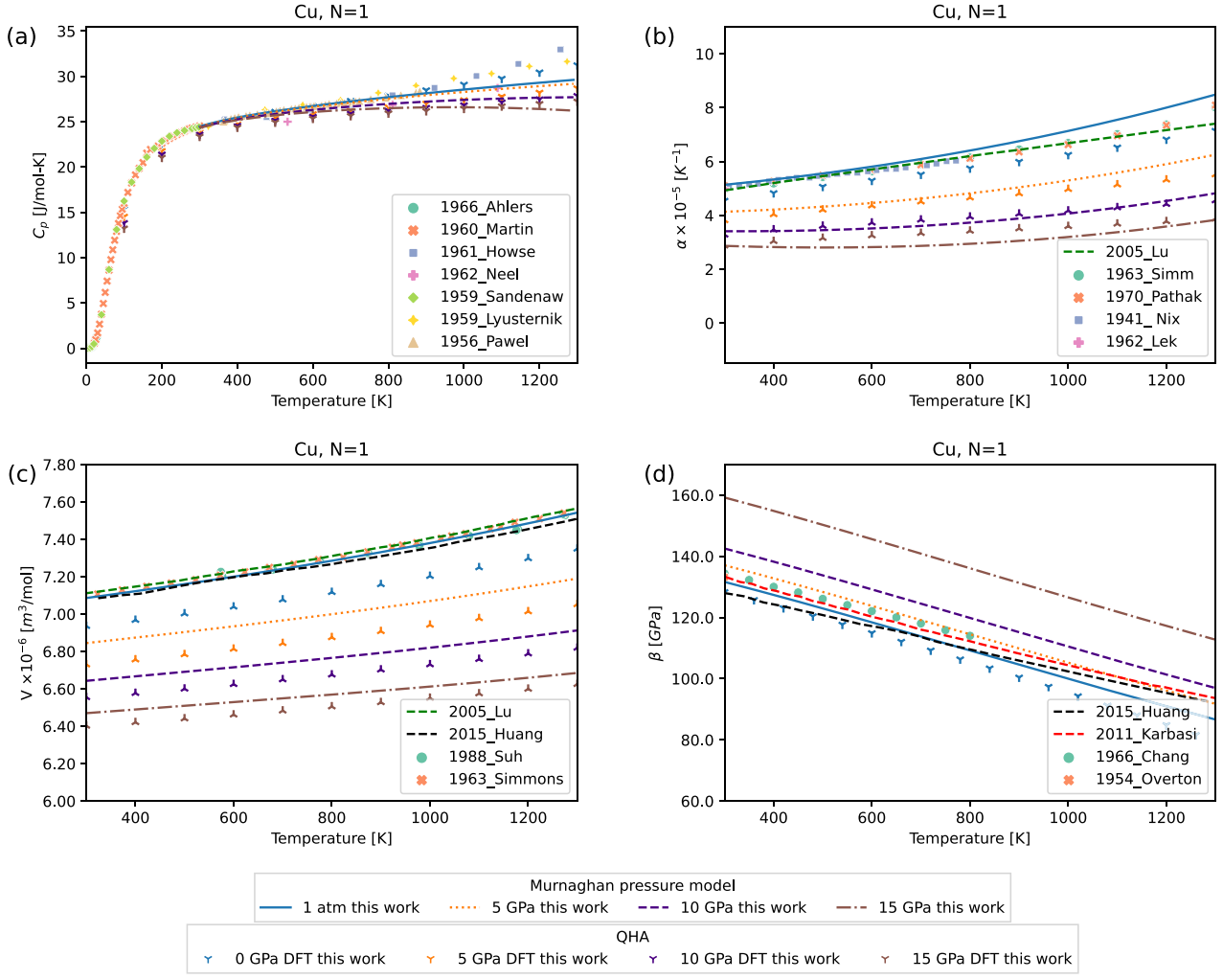

Fig. 8. Temperature-dependent thermophysical properties of FCC Cu determined using the Murnaghan pressure model and QHA calculations at various pressures: (a) Specific heat capacity at constant pressure (C_p), with literature data measured at 1 atm [100–106]. (b) Volumetric thermal expansion (α), compared to literature data at 1 atm [50,52,68,69,107]. (c) Measured molar volume, where the literature data is taken from Refs. [26,68,72,107]. (d) Bulk modulus (β) as a function of temperature, with data measured at atmospheric pressure [26,70,71,108].

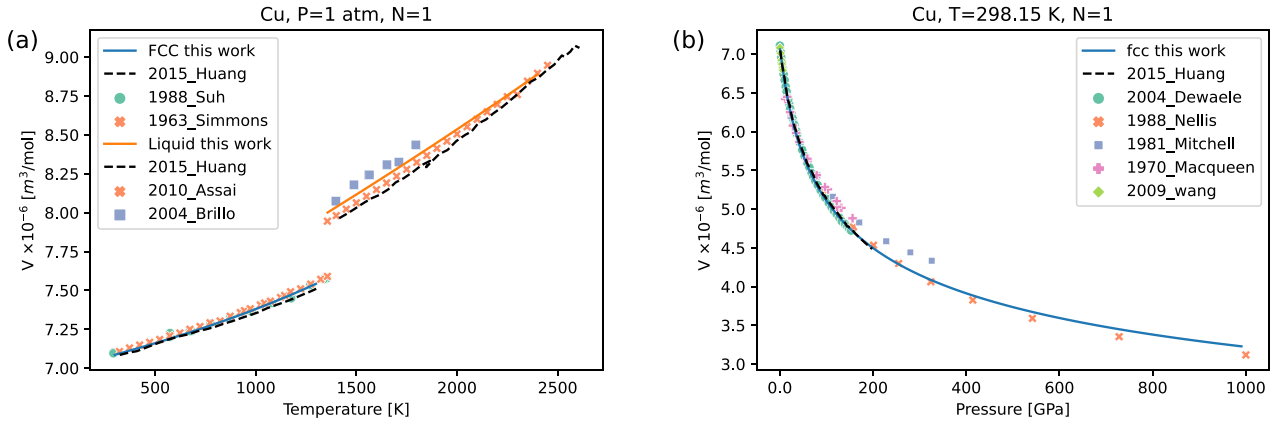

Fig. 9. Thermodynamic properties of unary Cu: (a) Calculated molar volume at room temperature with literature data [26,46,55,66,75,76]. (b) Measured molar volume as a function of temperature at atmospheric pressure, where the literature data is taken from Refs. [26,68,72–74].

theoretical [26,107] works. The QHA volume is somewhat underestimated for varying pressures because the approximation assumes that volume is dependent only on phonon frequencies, but temperature-dependent energies are not taken into account in the computation. Fig. 8 (d) shows the temperature dependence of β. There is a strong agreement between the computed β and other works [26,70,71,108].

For the FCC and liquid Cu phases, the molar volume is depicted as a function of temperature up to 2700 K in Fig. 9 (a). The computation from the current work coincides well with the experimental and theoretical findings [68,72–74] for both phases. Fig. 9 (b) shows the molar volume as a function of pressure. The results obtained from the present work agree well with the experimental results [46,55,66,75,76] and also with the work of Huang et al. [26].

4.3. Li unary system

The P-T diagram for Li constructed using the evaluated thermodynamic functions from Tables 1 and is shown in Fig. 10 overlaid with data from the existing works [109–112]. The computed triple point is found at 513 K and 7.5 GPa, which is reasonably consistent with literature data [111,112] up to 15 GPa.

The specific heat capacity at constant pressure is displayed in Fig. 11 (a), which is in good agreement with the experimental results [92,98,99]. Tests were conducted on the Murnaghan pressure model under various pressures. As the pressure increases, the C_p decreases. In the QHA computation, this pattern is noted as well. The volumetric thermal expansion at atmospheric pressure is shown in Fig. 11 (b) with reference to the literature [95–97]. The pressure model exhibits a drop in α at higher pressures, which is consistent with the QHA estimate. Nevertheless, as compared to QHA, the model somewhat underestimates the thermal expansion at 1.5 GPa. However, the model could predict the steady increment of thermal expansion as a function of temperature similar to the QHA model. The volume for the BCC Li phase fluctuates as a function of time under various pressures, as seen in Fig. 11 (c). The experimental work [92] was compared with the model. Additionally, a comparison is presented between the molar volume and thermal expansion of the model and the theoretically calculated values obtained by Hallstedt [85], where the molar volume was directly represented as a function of temperature. A good agreement is shown between the isothermal bulk modulus shown in Fig. 11 (d) and the experimental work [92,98,99]. There is a positive correlation between pressure and bulk modulus.

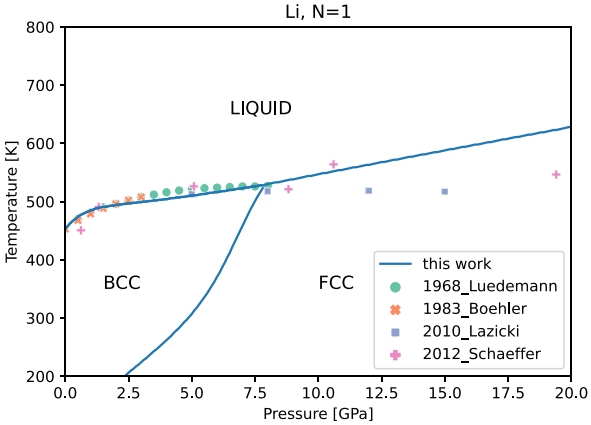

Fig. 10. Li pressure-temperature phase diagram obtained using the evaluated thermodynamic data from Table 1. Symbols indicate the corresponding literature data [109–112].

The assessed molar volume at 1 atm as a function of temperature and as a function of pressure at room temperature is well described in Fig. 12 (a) and (b), using experimental and theoretical data [92–94,116,117]. Overall, the present thermodynamic assessment leads to excellent agreement with available data from the literature, which is very scarce in terms of Li.

5. Conclusion

The optimized phase diagrams for all three unary systems (Al, Cu, Li) are reasonably close to existing experimental and computed data. The calculated property diagrams of the molar volume vs. pressure, volume vs. temperature, isothermal bulk modulus vs. temperature, and volumetric thermal expansion vs. temperature for Al, Cu, and Li systems are consistent with reported literature data, ensuring the accuracy of the phase diagrams. For the unary Al phase diagram, a better agreement with the work of Hänstrom et al. [62] is obtained up to 30 GPa. Cu phase diagram also shows good agreement with the experimental results. In case of Li phase diagram, the triple point was found at 7.5 GPa and the phase diagram is consistent with the experimental findings. For Al, Cu, and Li, the pressure model was used to determine the thermophysical parameters (bulk modulus, specific heat, and thermal expansion) at high pressure as a function of temperature. Furthermore, results are compared with QHA using phonon calculations and density functional theory at various pressures, showing excellent agreement.

The data obtained is pivotal for the development of binary Al–Cu and Al–Li systems. Its significance extends to serving as a crucial input parameter for kinetic modeling and phase-field simulations, particularly in the context of microstructure evolution at high pressures. The assessment is imperative for experimentalists to strategically choose compositions for non-equilibrium processes.

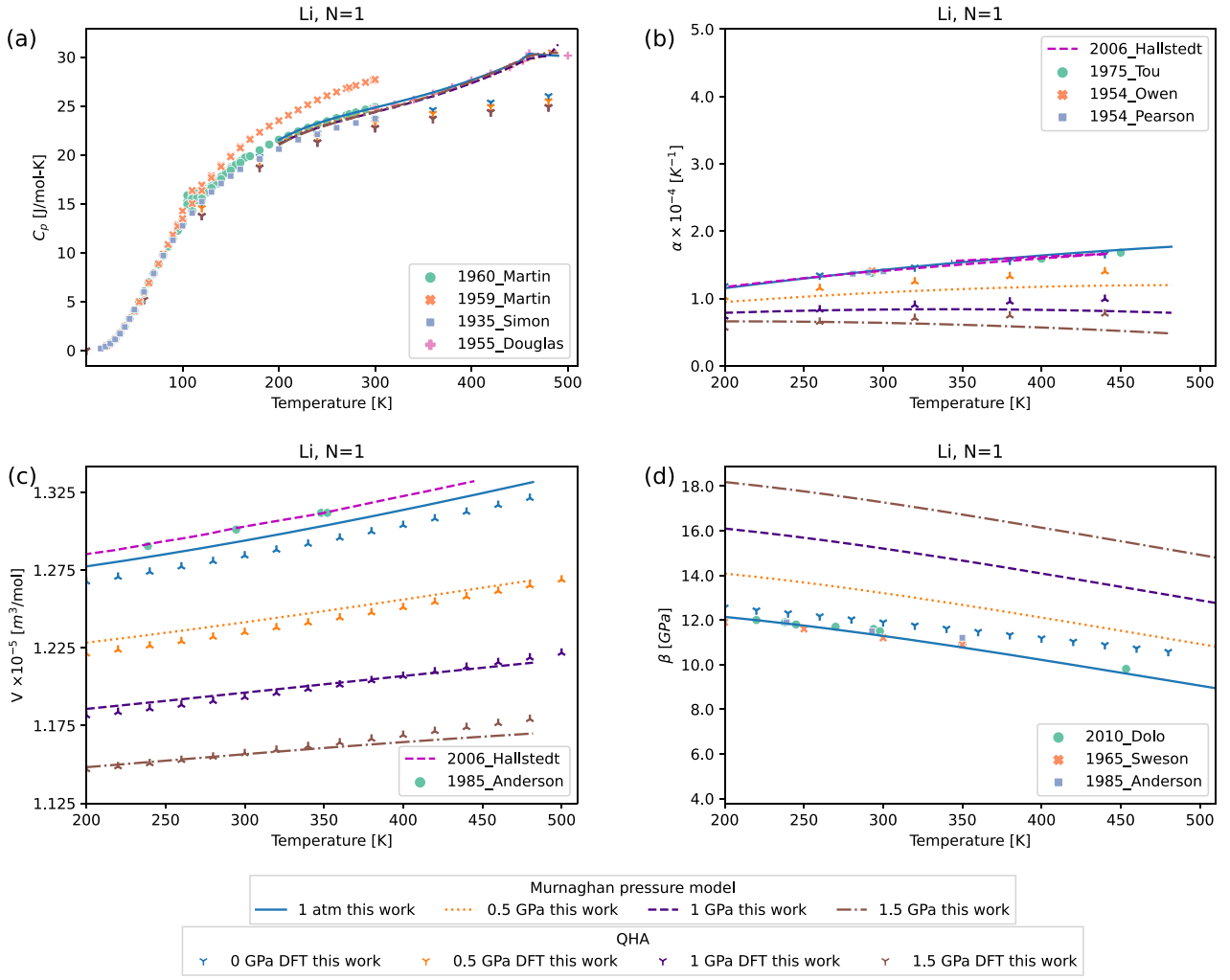

Fig. 11. Temperature-dependent thermophysical properties of BCC Li determined using the Murnaghan pressure model and QHA calculations at various pressures: (a) Specific heat capacity at constant pressure (C_p), with literature data measured at 1 atm [101,113–115]. (b) Volumetric thermal expansion (α), compared to literature data at 1 atm [85,95–97]. (c) Measured molar volume, where the literature data is taken from Refs. [85,92]. (d) Bulk modulus (β) as a function of temperature, with data measured at atmospheric pressure [92,98,99].

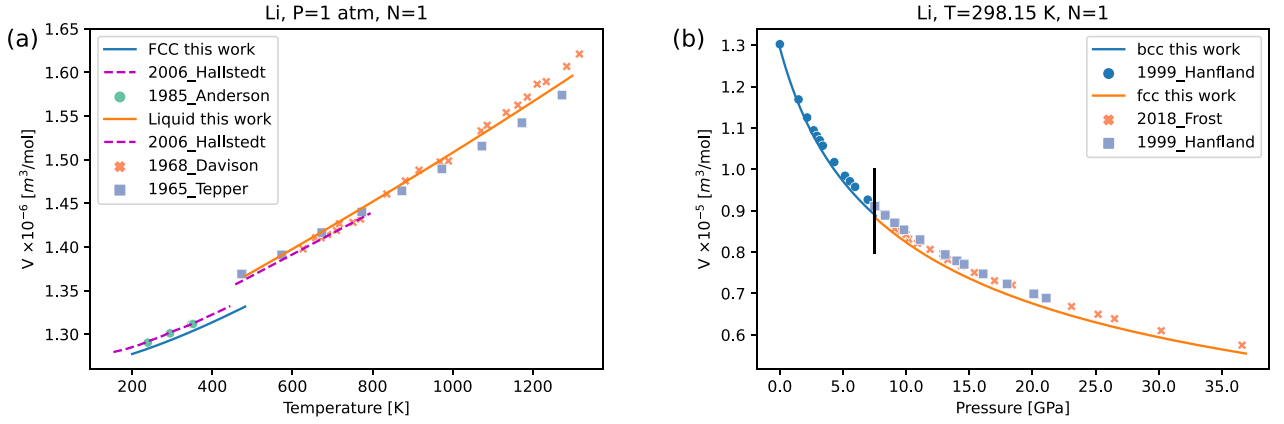

Fig. 12. Thermodynamic properties of unary Li: (a) Measured molar volume as a function of temperature at atmospheric pressure, where the literature data is taken from Refs. [85,92,116,117]. (b) Calculated molar volume at room temperature, with literature data [93,94].

Funding

This project has received funding from the European Research Council (ERC) under the European Union's Horizon 2020 research and innovation programme (grant agreement No 101001567).

CRediT authorship contribution statement

Elizabeth Mathew: Writing – original draft, Validation, Methodology, Conceptualization. **Rupesh Chafle:** Writing – review & editing, Supervision. **Benjamin Klusemann:** Writing – review & editing, Supervision, Funding acquisition, Conceptualization.

Declaration of competing interest

The authors declare that they have no known competing financial interests or personal relationships that could have appeared to influence the work reported in this paper.

Data availability

Supplementary data to this article can be found online at https://doi.org/10.1016/j.calphad.2024.102692.

Appendix A

A.1 Steps to obtain Eq. (3)

The standard thermodynamic formulation for thermal expansion serves as a starting point to calculate volume as a function of temperature $V(T, 1)$,

$$\alpha = \frac{1}{V}\left[\frac{\partial V}{\partial T}\right]_P,$$

Rearranging the equation

$$\int_{298.15}^{T} \alpha \, \mathrm{d}T = \int_{V_0}^{V(T,1)} \frac{1}{V} \, \mathrm{d}V,$$

Integrating

$$\int_{298.15}^{T} \alpha \, \mathrm{d}T = \ln \frac{V(T,1)}{V_0},$$

$$V(T,1) = V_0 \, \exp\left(\int_{298.15}^{T} \alpha(T,1) dT \right). \tag{A.1}$$

A.2 Steps to obtain Eq. (4)

Eq. (5) has already been written as,

$$G(T,P) = G(T,1) + V(T,1)\frac{[1 + nP\kappa(T)]^{1-\frac{1}{n}} - 1}{[n-1]\kappa(T)}. \tag{A.2}$$

Substituting the value of G from Eq. A.2 to the thermodynamic relation $V = \left[\frac{\partial G}{\partial P}\right]_T$ leads to,

$$\begin{aligned} V &= \frac{\mathrm{d}G(T,1)}{\mathrm{d}P} + \frac{V(T,1)}{[n-1]\kappa(T)} \cdot \frac{\mathrm{d}\left\{ [1 + nP\kappa(T)]^{1-\frac{1}{n}} - 1 \right\}}{\mathrm{d}P}, \\ &= \frac{V(T,1)}{[n-1]\kappa(T)} \cdot \frac{\mathrm{d}[1 + nP\kappa(T)]^{1-\frac{1}{n}}}{\mathrm{d}P}, \text{Chain rule} \\ &= \frac{V(T,1)}{\kappa(T)} \cdot \frac{[1 + nP\kappa(T)]^{-\frac{1}{n}}}{n} \cdot \frac{\mathrm{d}[1 + nP\kappa(T)]}{\mathrm{d}P}, \\ &= V(T,1)[1 + nP\kappa(T)]^{-\frac{1}{n}}. \end{aligned} \tag{A.3}$$

A.3 Steps to obtain G(T, P) (Eq. (5))

Eq. (1) is integrated after substituting the volume term from Eq. (2) that is obtained directly from the Murnaghan EOS. Rewriting those equations to show the proof leads to,

$$G(T,P) = G(T,1) + \int_1^P V(T,P)\,\mathrm{d}P. \tag{1}$$

$$V(T,P) = V(T,1)[1 + nP\kappa(T)]^{-\frac{1}{n}}. \tag{2}$$

Substituting Eq. (2) in second part of Eq. (1) that includes the pressure term, Then,

$$\int_1^P V(T,P)\,\mathrm{d}P = V(T,1)\int_1^P [1 + nP\kappa(T)]^{-\frac{1}{n}}\,\mathrm{d}P,$$

Substituting, $1 + nP\kappa(T) = x$

$$= V(T,1)\int_{P=1}^{P=P} \frac{x^{-\frac{1}{n}}\,\mathrm{d}x}{n\kappa(T)},$$

$$= V(T,1)\left[\frac{x^{1-\frac{1}{n}}}{[n-1]\kappa(T)}\right]_{P=1}^{P=P}, \text{Replace } x \;\&\; n\kappa(T) \sim 0 \tag{A.4}$$

$$= V(T,1)\frac{[1 + nP\kappa(T)]^{1-\frac{1}{n}} - 1}{[n-1]\kappa(T)}.$$

The assumption of $n\kappa(T) \sim 0$ is valid the n takes a value less than 5 for metals. Moreover, the compressibility values are of the order of 10^{-11} which is an extremely small value.

A.4 MD E-V curve for stable phase of unary alloys

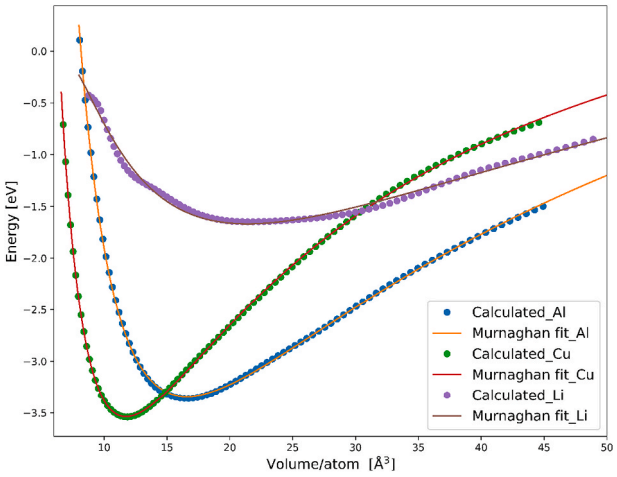

Fig. 13. E-V curve for Al, Cu and Li.

A.5 Divergence of heat capacity

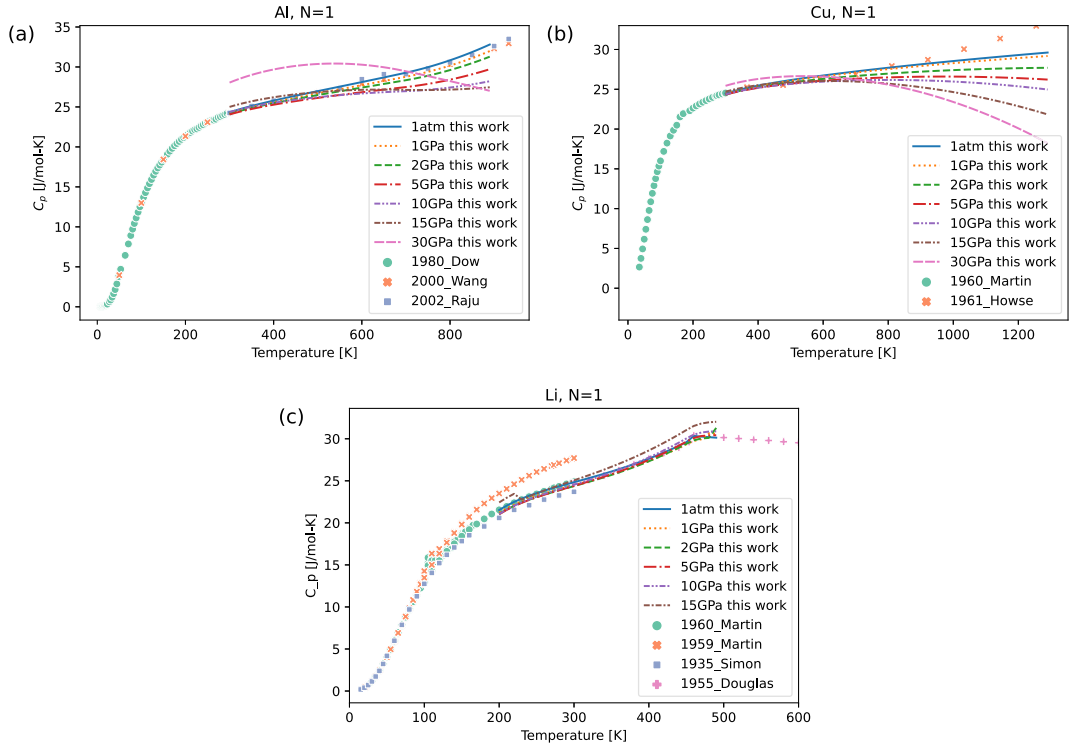

Fig. 14. Divergence of heat capacity for higher pressure in (a) Al (b) Cu (c) Li. Symbols indicate the corresponding literature data [54,55,84,101,102,113–115].

Murnaghan EOS assumes that the isothermal bulk modulus is linearily proportional to pressure. However, it has been reported it breaks down for for higher compression ranges [16].

A detailed description of the work can be seen in the supplementary.zip folder test_cp for Al. Inside the folder the specific database for every conditions that has been described in the python notebook test_cp.ipynb has also been included. The discussion about the C_p behaving differently has been discussed in the python notebook itself.

Appendix B. Supplementary data

Supplementary data to this article can be found online at https://doi.org/10.1016/j.calphad.2024.102692.

References

[1] J. Glazer, S.L. Verzasconi, E.N.C. Dalder, W. Yu, R.A. Emigh, R.O. Ritchie, J. W. Morris, Cryogenic Mechanical Properties of Al-Cu-Li-Zr Alloy 2090, Springer, 1986.
[2] N Eswara Prasad, T.R. Ramachandran, Phase diagrams and phase reactions in Al–Li alloys, in: Aluminum-lithium Alloys, Elsevier, 2014, pp. 61–97.
[3] J. Enz, C. Carrarin, S. Riekehr, V. Ventzke, N. Kashaev, Hot cracking behaviour of an autogenously laser welded Al-Cu-Li alloy, Int. J. Adv. Des. Manuf. Technol. 95 (1) (2018) 299–310.
[4] Jannik Goebel, Martin Reimann, Jorge F. dos Santos, Influence of Cu/Li ratio on the welding forces and mechanical properties of two Bobbin tool friction stir welded Al-Cu-Li alloys, J. Mater. Eng. Perform. 27 (10) (2018) 5212–5219.
[5] Enrique J. Lavernia, Nicholas J. Grant, Aluminium-lithium alloys, J. Mater. Sci. 22 (1987) 1521–1529.
[6] N Eswara Prasad, Amol Gokhale, Russell JH. Wanhill, Aluminum-lithium Alloys: Processing, Properties, and Applications, Butterworth-Heinemann, 2013.
[7] R.T. Chen, Jr Starke, EA, Microstructure and mechanical properties of mechanically alloyed, ingot metallurgy and powder metallurgy Al Li Cu Mg alloys, Mater. Sci. Eng. 67 (2) (1984) 229–245.
[8] D. Webster, G. Wald, W.S. Cremens, Mechanical properties and microstructure of argon atomized aluminum-lithium powder metallurgy alloys, Metall. Mater. Trans. 12 (1981) 1495–1502.
[9] M.A. Munoz-Morris, David G. Morris, Severe plastic deformation processing of Al–Cu–Li alloy for enhancing strength while maintaining ductility, Scripta Mater. 63 (3) (2010) 304–307.
[10] N Eswara Prasad, A.A. Gokhale, Rao, P. Rama, Mechanical behaviour of aluminium-lithium alloys, Sadhana 28 (2003) 209–246.
[11] A. Matsumuro, K. Sakai, M. Senoo, High-pressure phase diagram of an aluminium-rich Al-Li alloy at a pressure of 5.4 GPa, J. Mater. Sci. 28 (24) (1993) 6567–6570.
[12] P. Perrot, A to Z of thermodynamics, Supplement. Series 27 (1998).
[13] Francis Dominic Murnaghan, The compressibility of media under extreme pressures, Proc. Natl. Acad. Sci. USA 30 (9) (1944) 244–247.
[14] Pascal Vinet, John R. Smith, John Ferrante, James H. Rose, Temperature effects on the universal equation of state of solids, Phys. Rev. B 35 (4) (1987) 1945.
[15] Francis Birch, Finite elastic strain of cubic crystals, Phys. Rev. 71 (11) (1947) 809.
[16] A Fernández Guillermet, Per Gustafson, An assessment of the thermodynamic properties and the(p, T) phase diagram of iron, High Temp. 16 (6) (1984) 591–610. –High Press.
[17] Yongxin Ruan, Changrong Li, Chengliang Xu, Cuiping Guo, Zhenmin Du, Thermodynamic assessment of Mg/Zr unary systems, Comput. Mater. Sci. 154 (2018) 355–364.
[18] Xiao-Gang Lu, Malin Selleby, Bo Sundman, Implementation of a new model for pressure dependence of condensed phases in Thermo-Calc, Calphad 29 (1) (2005) 49–55.
[19] Bo Sundman, H.L. Lukas, S.G. Fries, Computational Thermodynamics: the Calphad Method, Cambridge university press Cambridge, 2007.
[20] Jean-Marc Joubert, Jean-Claude Crivello, G. Deffrennes, Modification of Lu's (2005) high pressure model for improved high pressure/high temperature extrapolations. Part I: modeling of platinum at high pressure/high temperature, Calphad 74 (2021) 102304.
[21] Eli Brosh, Guy Makov, Roni Z. Shneck, Application of CALPHAD to high pressures, Calphad 31 (2) (2007) 173–185.
[22] Eli Brosh, Roni Z. Shneck, Guy Makov, Explicit Gibbs free energy equation of state for solids, J. Phys. Chem. Solid. 69 (8) (2008) 1912–1922.
[23] G. Mie, Zur kinetischen theorie der einatomigen körper, Ann. Phys. 316 (8) (1903) 657–697.
[24] Xuantong Liu, Katsunari Oikawa, Assessment of temperature and pressure dependence of molar volume and phase diagrams of binary Al–Si Systems, Mater. Trans. 55 (11) (2014) 1673–1682.

[25] X. Liu, K. Oikawa, Assessment of the temperature and pressure dependence of molar volume and phase diagrams of cu and zn, Calphad 47 (2014) 114–122.
[26] Dandan Huang, Shuhong Liu, Yong Du, Bo Sundman, Modeling of the molar volume of the solution phases in the Al–Cu–Mg system, Calphad 51 (2015) 261–271.
[27] Z.-K. Liu, Y. Wang, S.-L. Shang, Zentropy theory for positive and negative thermal expansion, J. Phase Equilibria Diffus. 43 (6) (2022) 598–605.
[28] Alan T. Dinsdale, SGTE data for pure elements, Calphad 15 (4) (1991) 317–425.
[29] Richard Otis, Zi-Kui Liu, Pycalphad: CALPHAD-based computational thermodynamics in Python, J. Open Res. Software 5 (1).
[30] B. Hallstedt, N. Dupin, M. Hillert, L. Höglund, H.L. Lukas, J.C. Schuster, N. Solak, Thermodynamic models for crystalline phases. composition dependent models for volume, bulk modulus and thermal expansion, Calphad 31 (1) (2007) 28–37.
[31] G. Deffrennes, P. Faure, F. Bottin, J.-M. Joubert, B. Oudot, Tin (sn) at high pressure: review, x-ray diffraction, dft calculations, and gibbs energy modeling, J. Alloys Compd. 919 (2022) 165675.
[32] Ask Hjorth Larsen, Jens Jørgen Mortensen, Jakob Blomqvist, Ivano E. Castelli, Rune Christensen, Marcin Dułak, Jesper Friis, Michael N. Groves, Bjørk Hammer, Cory Hargus, The atomic simulation environment—a Python library for working with atoms, J. Phys. Condens. Matter 29 (27) (2017) 273002.
[33] Peter E. Blöchl, Projector augmented-wave method, Phys. Rev. B 50 (24) (1994) 17953.
[34] John P. Perdew, Kieron Burke, Matthias Ernzerhof, Generalized gradient approximation made simple, Phys. Rev. Lett. 77 (18) (1996) 3865.
[35] Hendrik J. Monkhorst, James D. Pack, Special points for Brillouin-zone integrations, Phys. Rev. B 13 (12) (1976) 5188.
[36] Atsushi Togo, First-principles phonon calculations with phonopy and Phono3py, J. Phys. Soc. Jpn. 92 (1) (2023) 012001.
[37] Martin T. Dove, Introduction to Lattice Dynamics, vol. 4, Cambridge university press, 1993.
[38] Togo, Atsushi and Tanaka, Isao, First principles phonon calculations in materials science, Scripta Mater. 108 (2015) 1–5.
[39] Murray S. Daw, Michael I. Baskes, Embedded-atom method: derivation and application to impurities, surfaces, and other defects in metals, Phys. Rev. B 29 (12) (1984) 6443.
[40] Y. Mishin, Diana Farkas, M.J. Mehl, D.A. Papaconstantopoulos, Interatomic potentials for monoatomic metals from experimental data and ab initio calculations, Phys. Rev. B 59 (5) (1999) 3393.
[41] Yu Mishin, M.J. Mehl, D.A. Papaconstantopoulos, A.F. Voter, J.D. Kress, Structural stability and lattice defects in copper: ab initio, tight-binding, and embedded-atom calculations, Phys. Rev. B 63 (22) (2001) 224106.
[42] Alan Nichol, Graeme J. Ackland, Property trends in simple metals: an empirical potential approach, Phys. Rev. B 93 (18) (2016) 184101.
[43] Michael J. Tambe, Nicola Bonini, Nicola Marzari, Bulk aluminum at high pressure: a first-principles study, Phys. Rev. B 77 (17) (2008) 172102.
[44] G.V. Sin'Ko, N.A. Smirnov, Ab initio calculations of elastic constants and thermodynamic properties of bcc, fcc, and hcp Al crystals under pressure, J. Phys. Condens. Matter 14 (29) (2002) 6989.
[45] F. Jona, P.M. Marcus, Lattice parameters of aluminium in the Mbar range by first-principles, J. Phys. Condens. Matter 18 (48) (2006) 10881.
[46] W.J. Nellis, J.A. Moriarty, A.C. Mitchell, M. Ross, R.G. Dandrea, N.W. Ashcroft, N. C. Holmes, G.R. Gathers, Metals physics at ultrahigh pressure: aluminum, copper, and lead as prototypes, Phys. Rev. Lett. 60 (14) (1988) 1414.
[47] Y. Akahama, M. Nishimura, K. Kinoshita, H. Kawamura, Y. Ohishi, Evidence of a fcc-hcp transition in aluminum at multimegabar pressure, Phys. Rev. Lett. 96 (4) (2006) 045505.
[48] D.N. Polsin, D.E. Fratanduono, J.R. Rygg, A. Lazicki, R.F. Smith, J.H. Eggert, M. C. Gregor, B.H. Henderson, J.A. Delettrez, R.G. Kraus, others, Measurement of body-centered-cubic aluminum at 475 GPa, Phys. Rev. Lett. 119 (17) (2017) 175702.
[49] A.J.C. Wilson, The thermal expansion of aluminium: further experiments, Proc. Phys. Soc. 54 (6) (1942) 487.
[50] F.C. Nix, D. MacNair, The thermal expansion of pure metals: copper, gold, aluminum, nickel, and iron, Phys. Rev. 60 (8) (1941) 597.
[51] F.R. Kroeger, C.A. Swenson, Absolute linear thermal-expansion measurements on copper and aluminum from 5 to 320 K, J. Appl. Phys. 48 (3) (1977) 853–864.
[52] P.D. Pathak, N.G. Vasavada, Thermal expansion and the law of corresponding states, J. Phys. C Solid State Phys. 3 (2) (1970) L44.
[53] William Burton Pearson, A Handbook of Lattice Spacings and Structures of Metals and Alloys: International Series of Monographs on Metal Physics and Physical Metallurgy, vol. 4, Elsevier, 2013, 4.
[54] S. Raju, K. Sivasubramanian, E. Mohandas, The high temperature bulk modulus of aluminium: an assessment using experimental enthalpy and thermal expansion data, Solid State Commun. 122 (12) (2002) 671–676.
[55] Kai Wang, Robert R. Reeber, The perfect crystal, thermal vacancies and the thermal expansion coefficient of aluminium, Philos. Mag. A 80 (7) (2000) 1629–1643.
[56] J.L. Tallon, A. Wolfenden, Temperature dependence of the elastic constants of aluminum, J. Phys. Chem. Solid. 40 (11) (1979) 831–837.
[57] D. Gerlich, E.S. Fisher, The high temperature elastic moduli of aluminum, J. Phys. Chem. Solid. 30 (5) (1969) 1197–1205.
[58] Marc J. Assael, Konstantinos Kakosimos, R Michael Banish, Jürgen Brillo, Ivan Egry, Robert Brooks, Peter N. Quested, Kenneth C. Mills, Akira Nagashima, Yuzuru Sato, others, Reference data for the density and viscosity of liquid aluminum and liquid iron, J. Phys. Chem. Ref. Data 35 (1) (2006) 285–300.
[59] S.A. Yatsenko, V.I. Kononenko, A.L. Sukhman, Temperature dependence of surface tension and density of tin, indium, aluminum, and gallium, Teplofiz. Vysok. Temp. 10 (1) (1972) 66–71.
[60] Patrick M. Smith, John W. Elmer, Gilbert F. Gallegos, Measurement of the density of liquid aluminum alloys by an X-ray attenuation technique, Scripta Mater. 40 (8) (1999) 937–941.
[61] J. Lees, B.H.J. Williamson, Combined very high pressure/high temperature calibration of the tetrahedral anvil apparatus, fusion curves of zinc, aluminium, germanium and silicon to 60 kilobars, Nature 208 (1965) 278–279.
[62] A. Hänström, P. Lazor, High pressure melting and equation of state of aluminium, J. Alloys Compd. 305 (1–2) (2000) 209–215.
[63] Reinhard Boehler, Marvin Ross, Melting curve of aluminum in a diamond cell to 0.8 Mbar: implications for iron, Earth Planet Sci. Lett. 153 (3–4) (1997) 223–227.
[64] A. Jayaraman, Jr W. Klement, R.C. Newton, G.C. Kennedy, Fusion curves and polymorphic transitions of the group III elements—aluminum, gallium, indium and thallium—at high pressures, J. Phys. Chem. Solid. 24 (1) (1963) 7–18.
[65] K. Syassen, W.B. Holzapfel, Isothermal compression of Al and Ag to 120 kbar, J. Appl. Phys. 49 (8) (1978) 4427–4430.
[66] Agnes Dewaele, Paul Loubeyre, Mohamed Mezouar, Equations of state of six metals above 94 GPa, Phys. Rev. B 70 (9) (2004) 094112.
[67] Raymond G. Greene, Huan Luo, Arthur L. Ruoff, Al as a simple solid: high pressure study to 220 GPa (2.2 Mbar), Phys. Rev. Lett. 73 (15) (1994) 2075.
[68] R.O. Simmons, R.W. Balluffi, Measurement of equilibrium concentrations of vacancies in copper, Phys. Rev. 129 (4) (1963) 1533.
[69] G.K. White, Thermal expansion of reference materials: copper, silica and silicon, J. Phys. Appl. Phys. 6 (17) (1973) 2070.
[70] Y.A. Chang, L. Himmel, Temperature dependence of the elastic constants of Cu, Ag, and Au above room temperature, J. Appl. Phys. 37 (9) (1966) 3567–3572.
[71] Jr Overton, WC and Gaffney, John, Temperature variation of the elastic constants of cubic elements. I. Copper, Phys. Rev. 98 (4) (1955) 969.
[72] Suh In-Kook, H. Ohta, Y. Waseda, High-temperature thermal expansion of six metallic elements measured by dilatation method and X-ray diffraction, J. Mater. Sci. 23 (1988) 757–760.
[73] Marc J. Assael, Agni E. Kalyva, Konstantinos D. Antoniadis, Michael Banish R, Ivan Egry, Jiangtao Wu, Erhard Kaschnitz, William A. Wakeham, Reference data for the density and viscosity of liquid copper and liquid tin, J. Phys. Chem. Ref. Data 39 (3) (2010) 033105.
[74] Jürgen Brillo, Ivan Egry, Density and excess volume of liquid copper, nickel, iron, and their binary alloys, Int. J. Mater. Res. 95 (8) (2022) 691–697.
[75] A.C. Mitchell, W.J. Nellis, Shock compression of aluminum, copper, and tantalum, J. Appl. Phys. 52 (5) (1981) 3363–3374.
[76] R.G. McQueen, S.P. Marsh, J.W. Taylor, J.N. Fritz, W.J. Carter, The equation of state of solids from shock wave studies, High Velocity Imp. Phenomena 293 (1970) 294–417.
[77] Y. Wang, J. Zhang, H. Xu, Z. Lin, L. L. Daemen, Y. Zhao, L. Wang, Thermal Equation of State of Copper Studied by High P-T Synchrotron X-Ray Diffraction.
[78] Jagannadham Akella, George C. Kennedy, Melting of gold, silver, and copper—proposal for a new high-pressure calibration scale, J. Geophys. Res. 76 (20) (1971) 4969–4977.
[79] Peter W. Mirwald, George C. Kennedy, The melting curve of gold, silver, and copper to 60-Kbar pressure: a reinvestigation, J. Geophys. Res. Solid Earth 84 (B12) (1979) 6750–6756.
[80] H. Brand, D.P. Dobson, L. Vočadlo, I.G. Wood, Melting curve of copper measured to 16 GPa using a multi-anvil press, High Pres. Res. 26 (3) (2006) 185–191.
[81] F. Guinea, J.H. Rose, J.R. Smith, J. Ferrante, Scaling relations in the equation of state, thermal expansion, and melting of metals, Appl. Phys. Lett. 44 (1) (1984) 53–55.
[82] Y. Touloukian, E. Buyco, Thermophysical Properties of Matter-The Tprc Data Series. Volume 4. Specific Heat-Metallic Elements and Alloys, Thermophysical and Electronic Properties Information Analysis, Center Lafayette in.
[83] W. Giauque, P. Meads, The heat capacities and entropies of aluminum and copper from 15 to 300° k, J. Am. Chem. Soc. 63 (7) (1941) 1897–1901.
[84] D. Downie, J. Martin, An adiabatic calorimeter for heat-capacity measurements between 6 and 300 k. the molar heat capacity of aluminium, J. Chem. Therm. 12 (8) (1980) 779–786.
[85] B. Hallstedt, Molar volumes of al, li, mg and si, Calphad 31 (2) (2007) 292–302.
[86] J.B. Neaton, N.W. Ashcroft, Pairing in dense lithium, Nature 400 (6740) (1999) 141–144.
[87] Michael Hanfland, K. Syassen, N.E. Christensen, D.L. Novikov, New high-pressure phases of lithium, Nature 408 (6809) (2000) 174–178.
[88] Jian Lv, Yanchao Wang, Li Zhu, Yanming Ma, Predicted novel high-pressure phases of lithium, Phys. Rev. Lett. 106 (1) (2011) 015503.
[89] Takahiro Matsuoka, Katsuya Shimizu, Direct observation of a pressure-induced metal-to-semiconductor transition in lithium, Nature 458 (7235) (2009) 186–189.
[90] Yansun Yao, J.S. Tse, K. Tanaka, F. Marsiglio, Y. Ma, Superconductivity in lithium under high pressure investigated with density functional and Eliashberg theory, Phys. Rev. B 79 (5) (2009) 054524.
[91] Christophe L. Guillaume, Eugene Gregoryanz, Olga Degtyareva, Malcolm I. McMahon, Michael Hanfland, Shaun Evans, Malcolm Guthrie, Stanislav V. Sinogeikin, H.K. Mao, Cold melting and solid structures of dense lithium, Nat. Phys. 7 (3) (2011) 211–214.
[92] M.S. Anderson, C.A. Swenson, Experimental equations of state for cesium and lithium metals to 20 kbar and the high-pressure behavior of the alkali metals, Phys. Rev. B 31 (2) (1985) 668.

[93] Mungo Frost, Abraham L. Levitan, Peihao Sun, Siegfried Glenzer, Equation of state and electron localisation in fcc lithium, J. Appl. Phys. 123 (6) (2018) 065901.
[94] M. Hanfland, I. Loa, K. Syassen, U. Schwarz, K. Takemura, Equation of state of lithium to 21 GPa, Solid State Commun. 112 (3) (1999) 123–127.
[95] Yeram Sarkis Touloukian, R. K. Kirby, R. E. Taylor, P. D. Desai, Thermal Expansion: Metallic Elements and Alloys.
[96] E.A. Owen, G.I. Williams, X-ray measurements on lithium at low temperatures, Proc. Phys. Soc. 67 (10) (1954) 895.
[97] W.B. Pearson, Thermal expansion of lithium, 77° to 300° K, Can. J. Phys. 32 (11) (1954) 708–713.
[98] C.A. Swenson, Lithium metal: an experimental equation of state, J. Phys. Chem. Solid. 27 (1) (1966) 33–38.
[99] E. Dologlou, Self-diffusion in solid lithium, Glass Phys. Chem. 36 (2010) 570–574.
[100] G. Ahlers, Heat capacity of copper, Rev. Sci. Instrum. 37 (4) (1966) 477–480.
[101] D.L. Martin, The specific heat of sodium from 20 to 300 k: the martensitic transformation, Proc. Roy. Soc. Lond. Math. Phys. Sci. 254 (1279) (1960) 433–443.
[102] P.T. Howse, C. Pears, S. Oglesby, The Thermal Properties of Some Plastic Panels, Wright Air Development Division, Air Research and Development Command, 1961.
[103] D. S. Neel, C. D. Pears, J. R. Oglesby, The Thermal Properties of Thirteen Solid Materials to 5000 Degrees F for Their Destruction Temperatures, Souther Research Inst, Birmingham, AL, United States.
[104] T.A. Sandenaw, Heat Capacity of Copper below 300° K, a Test of Two Calorimeter Designs, vol. 2307, Los Alamos Scientific Laboratory of the University of California, 1959.
[105] V. Lyusternik, Automatic calorimeter for quantitative thermal analysis of heat resistant steels, Pribory Tekhn, Eksperim 4 (1959) 127–129.
[106] R. E. Pawel, The Application of Dynamic Adiabatic Calorimetry to the Copper-Nickel System from 50 to 620 C.
[107] X.-G. Lu, M. Selleby, B. Sundman, Assessments of molar volume and thermal expansion for selected bcc, fcc and hcp metallic elements, Calphad 29 (1) (2005) 68–89.
[108] A. Karbasi, S. Saxena, R. Hrubiak, The thermodynamics of several elements at high pressure, Calphad 35 (1) (2011) 72–81.
[109] H.D. Luedemann, G.C. Kennedy, Melting curves of lithium, sodium, potassium, and rubidium to 80 kilobars, J. Geophys. Res. 73 (8) (1968) 2795–2805.
[110] R. Boehler, Melting temperature, adiabats, and Grüneisen parameter of lithium, sodium and potassium versus pressure, Phys. Rev. B 27 (11) (1983) 6754.
[111] Amy Lazicki, Yingwei Fei, Russell J. Hemley, High-pressure differential thermal analysis measurements of the melting curve of lithium, Solid State Commun. 150 (13–14) (2010) 625–627.
[112] Anne Marie J. Schaeffer, William B. Talmadge, Scott R. Temple, Shanti Deemyad, High pressure melting of lithium, Phys. Rev. Lett. 109 (18) (2012) 185702.
[113] D.L. Martin, Specific heats of lithium isotopes from 20° to 300° k, Physica 25 (7–12) (1959) 1193–1199.
[114] F. Simon, R. Swain, Untersuchungen über die spezifischen wärmen bei tiefen temperaturen, Z. Phys. Chem. 28 (1) (1935) 189–198.
[115] T.B. Douglas, L.F. Epstein, J.L. Dever, W.H. Howland, Lithium: heat content from 0 to 900°, triple point and heat of fusion, and thermodynamic properties of the solid and liquid1, J. Am. Chem. Soc. 77 (8) (1955) 2144–2150.
[116] Harry W. Davison, Compilation of Thermophysical Properties of Liquid Lithium, vol. 4650, National Aeronautics and Space Administration, 1968.
[117] F. Tepper, J.S. Zelenak, F. Roehlich Jr, V.B. May, Thermophysical and transport properties of liquid metals. MSA research corp, Tech. Rep. AFFDL-TR (1965) 65–99. DE No. AD-464138.